SSC20-XII-07

A Comparison of Techniques for Non Data-Aided Carrier Tracking of Phase-Modulated Signals

Brendan Hill, Nazia Mozaffar, Salwan Damman
NIWC Pacific
53560 Hull Street, San Diego, CA 92152

ABSTRACT

Communications between ground stations and nanosats in low earth orbit (LEO) require acquisition and tracking of large Doppler frequency offsets due to the relative velocity the between the transmitter and the receiver. The Doppler frequency shift varies with time, reaching its fastest rate of change as the small satellite reaches its closest approach to the ground station. Non data-aided techniques for acquiring and tracking the carrier frequency offset without requiring the processing of symbols have been developed to address this problem. One technique is the use of a frequency-locked loop (FLL) comprised of band edge filters that convert the energy in the modulated signal's excess bandwidth into a control signal proportional to the frequency offset. Alternatively, the Doppler frequency offset, in addition to the modulation rate of a phase modulated signal, can be obtained by simply multiplying the incoming signal by itself or by a time-delayed version of itself. The frequency offset component of this processed signal can be extracted with a phase-locked loop (PLL) which filters the excess noise and removes the tones associated with the original signal's symbol modulation rate. This PLL filtered signal can then be used in a FLL to correct the observed time-varying Doppler frequency. This paper presents a comparison between these two techniques for BPSK signals in both high and low SNR environments, highlighting the advantages and disadvantages of each approach. MATLAB results for each tracker are shown with varying SNR, static Doppler, and dynamic Doppler frequency offset.

INTRODUCTION

Small satellites in low earth orbit can close communication links to ground terminals with less power than their counterparts in higher orbits by virtue of their closer distance. However, satellites in lower orbits travel at higher velocities, and thus are more susceptible to Doppler shift. For example, a satellite in a circular orbit 500 miles above the mean sea level of Earth will travel at 7.45 km/s in order to stay in orbit. If the satellite were travelling due west over Logan, UT, and if a ground terminal were located directly under the flight path of the satellite, the satellite would observe a time-varying Doppler frequency offset from the ground terminal according to the graph shown in Figure 1. In this simple example, the Doppler starts at nearly 57 kHz, changing very little until three minutes before zenith, at which time it decreases rapidly, reaching -57 kHz at three minutes after zenith. The maximum frequency change occurs just as the satellite passes overhead (at t=0), when the Doppler changes by -550 Hz/s, as seen in Figure 2. A means of detecting and tracking a time-changing Doppler frequency without having to demodulate the signal would simplify the receiver design. Alternatively, such a correction technique could allow the satellite to function as an in-orbit relay station, correcting an observed Doppler and re-transmitting the signal pre-distorted with a Doppler profile that negates what the next relay node would observe. Two methods of Doppler detection are discussed in this paper. Both methods involve the manipulation of the incoming signal energy to create a new signal that contains a spectral tone, and using this in a feedback control loop to drive the frequency error to zero.

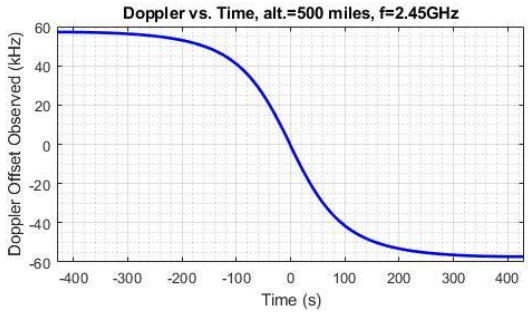

Figure 1: Doppler vs. Time (500 Mile Satellite Altitude, 2.45 GHz, overhead at t=0)

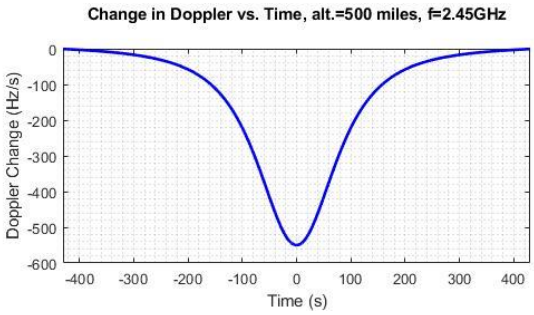

Figure 2: Change in Doppler vs. Time (500 Mile Satellite Altitude, 2.45 GHz, overhead at t=0)

BAND EDGE FILTERS

Background

Phase modulated signals are filtered in order to contain the spectrum so that bandwidth can be shared among multiple channels. The receiver has a copy of this

baseband filter (the "matched filter") and uses it to maximize the signal to noise ratio of the received signal. If extra filters are located at the positive and negative edges of the channel, the relative energy received from the filters can be used to determine the frequency offset of the modulated signal. This energy difference can be fed to a feedback control loop, which will automatically minimize the Doppler offset. This is the band edge filter approach described by Harris[1]. In his derivation of the optimum band edge filter, Harris shows that its magnitude frequency response is the derivative (with respect to frequency) of the matched filter's frequency response. Band edge filters are symmetrically situated at the positive and negative ends of the baseband signal spectrum, located at $\pm(1+\alpha)f_{sym}/2$, where α is the rolloff in the Nyquist shaping filter and f_{sym} is the symbol rate. As an example, Figure 3 and Figure 4 show the spectra of the band edge filters (and their associated matched filters) for a system designed for a signal with a 50 kHz modulation rate. The rolloff factor α is zero for Figure 3, and the band edge filters are centered at ±25 kHz. The α factor is unity for Figure 4, and the band edge filters are centered at ±50 kHz. For clarity, the horizontal axis has been set to the limits of ±100 kHz even though the sample rate used in generating the figures was 1 MS/s. In the figures, there are 201 coefficients in each band edge filter and the matched filter.

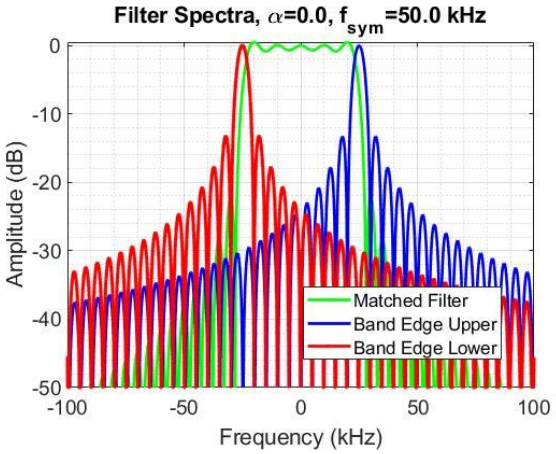

Figure 3: Band Edge and Matched Filter Spectra, α = 0, f_{sym} = 50 kHz, 201 Coefficients

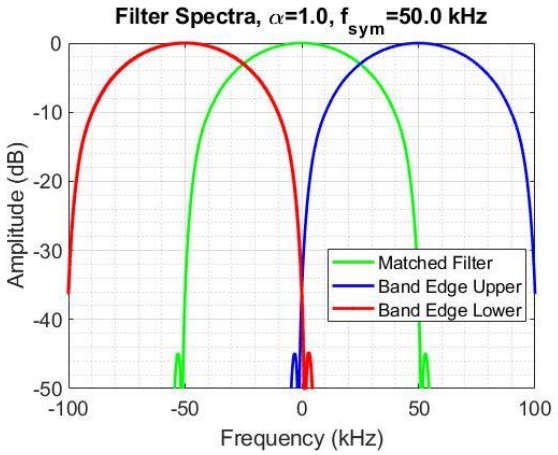

Figure 4: Band Edge and Matched Filter Spectra, α = 1, f_{sym} = 50 kHz, 201 Coefficients

Note that the band edge filters have very narrow bandwidth for the α = 0 case, and a bandwidth roughly equal to the matched filter bandwidth for α = 1. In fact, the bandwidth of the α = 0 band edge filters diminishes as the number of coefficients increases. This illustrates the fact that the optimum band edge filters operate on the excess bandwidth of the incoming signal.[1]

Harris introduces an implementation that calculates the band edge filter energy difference using the sum and difference of the band edge filter outputs[1]. Let the positive frequency band edge filter's baseband output be defined as *a(t)*, and let the negative filter's baseband output be defined as *b(t)*. The upper and lower band edge filter outputs are expressed as in (1).

$$be_{upper}(t) = a(t)e^{\frac{j2\pi(1+\alpha)f_{sym}t}{2}} \qquad (1)$$

$$be_{lower}(t) = b(t)e^{\frac{-j2\pi(1+\alpha)f_{sym}t}{2}}$$

In (2), we define the sum of the band edge filters as *cc(t)*, and the difference between the upper and lower band edge filters as *ss(t)*.

$$cc(t) = a(t)e^{\frac{j2\pi(1+\alpha)f_{sym}t}{2}} + b(t)e^{\frac{-j2\pi(1+\alpha)f_{sym}t}{2}} \qquad (2)$$
$$ss(t) = a(t)e^{\frac{j2\pi(1+\alpha)f_{sym}t}{2}} - b(t)e^{\frac{-j2\pi(1+\alpha)f_{sym}t}{2}}$$

The product of *cc(t)* with the conjugate of *ss(t)* produces a complex sum whose real part is equal to the difference in energy received in the band edge filters.

$$cc(t)\cdot ss^*(t) = (|a(t)|^2 - |b(t)|^2) + \left(a^*(t)b(t)e^{-j2\pi(1+\alpha)f_{sym}t} - a(t)b^*(t)e^{j2\pi(1+\alpha)f_{sym}t}\right) \qquad (3)$$

The second term in parenthesis in (3) is the difference between a complex number and its conjugate, which produces a strictly imaginary term. A demonstration of the output spectra of the band edge filters as well as the real part of the signal in (3) is shown in Figure 5 with noise removed for clarity. The figure depicts a Doppler frequency offset of 12.5 kHz for a BPSK signal modulated at 50 kHz and a rolloff factor of 0.5. Note that the spectrum of the real part of $cc(t)ss^*(t)$ contains a tone at DC. Its amplitude is proportional to the difference in the band edge filters' energies.

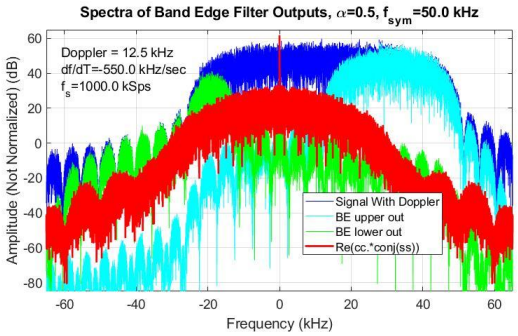

Figure 5: Example Spectra of Band Edge Filter Outputs

Incorporation of Band Edge Filters into FLL

Figure 6 shows a block diagram of a frequency locked loop (FLL) using band edge filters. This implementation computes the real part of the product of *cc(t)* and *ss*(t)*, filters it with a proportional and integral filter, and drives a numerically controlled oscillator (NCO) with the result. The NCO output is conjugated and then multiplied by the incoming signal, completing the feedback path and cancelling the Doppler offset.

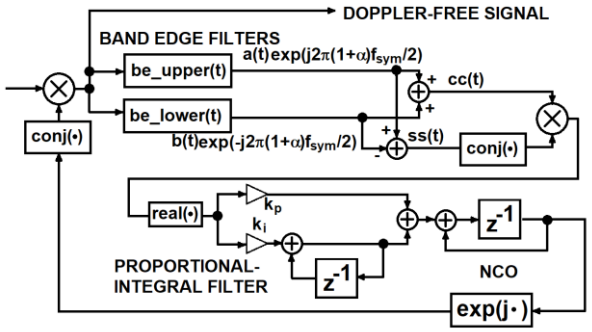

Figure 6: Band Edge Filter Frequency Locked Loop Structure

The proportional and integral path constants are computed by selecting the loop bandwidth parameter η, choosing a damping factor ζ, and substituting these parameters into equation (4).

$$k_p = \frac{4\zeta\eta}{1+2\zeta\eta+\eta^2} \qquad (4)$$

$$k_i = \frac{4\eta^2}{1+2\zeta\eta+\eta^2}$$

The expressions for k_p and k_i shown in (4) are the same values that are used in a generic second-order phase locked loop, and they are briefly derived in the Appendix.

Performance of Band Edge Filter FLL

A MATLAB simulation of an FLL system with the diagram of Figure 6 using α = 0.5, $\zeta = 1/\sqrt{2}$ and $\eta = 2\pi/200$ is shown in Figure 7 (20 dB SNR) and Figure 8 (5 dB SNR). In each graph, the incoming BPSK signal is modulated at a symbol rate 50 kHz, the Doppler offset starts at 12.5 kHz, and the Doppler frequency decreases by 550 Hz/s. The sample rate used is 1 MS/s.

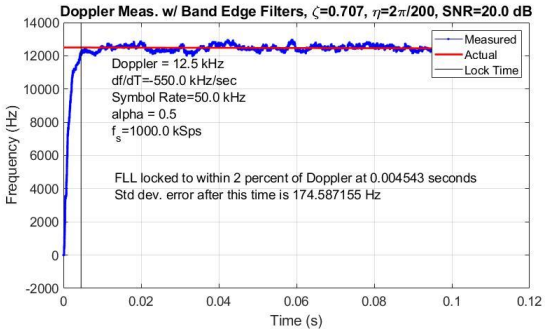

Figure 7: Performance of Band Edge Filter FLL at SNR = 20 dB

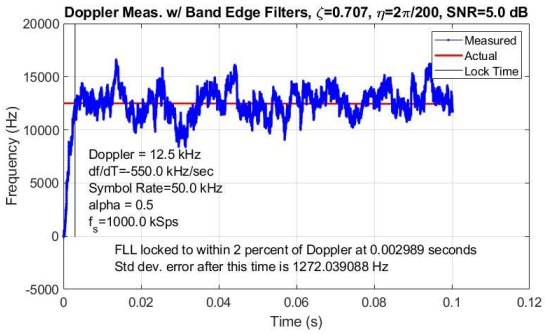

Figure 8: Performance of Band Edge Filter FLL at SNR = 5 dB

The frequency measurements are obtained by monitoring the output of the NCO accumulator. Figure 8 shows a much wider variation of the measured frequency about the true frequency when compared to Figure 7, and this is due to the SNR in the operating environment. This could be alleviated by narrowing the loop bandwidth parameter, but this would slow down the response time of the FLL. Figure 9 shows that when η is reduced by a

factor of 10, the variation of the measured frequency closely tracks the actual frequency, but the system takes more than 100 times longer to acquire the signal. The simulation was extended in time from 100,000 points (Figure 8) to 2,000,000 points (Figure 9). With this extended simulation time, the -550 Hz/s change in Doppler frequency vs. time is easier to observe.

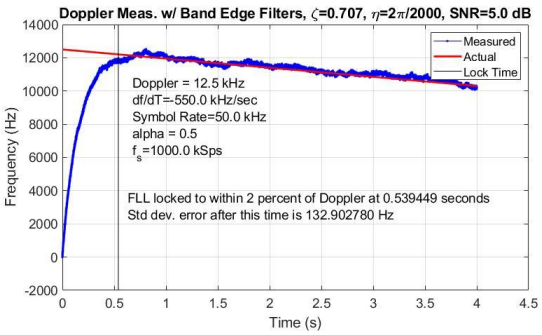

Figure 9: Performance of Band Edge Filter FLL at SNR = 5 dB with Reduced Loop Bandwidth

Advantage of Optimum Band Edge FLL

The optimum band edge filter design maximizes the correlated energy with respect to frequency. This design is determined strictly from the shaping filter used on the original baseband data, which in turn is parameterized strictly from the rolloff factor and symbol rate. If the modulation type is changed to any type that includes phase modulation, such as QPSK, Offset QPSK, 8PSK, or even QAM-16, the shaping filters and hence the band edge filters are unchanged.

Disadvantage of Optimum Band Edge FLL

If the magnitude of the Doppler frequency of the incoming band edge filter is large enough, its main lobe will not line up with either of the band edge filters. Only the sidelobes of the band edge filters will collect energy, and the difference between them will be nearly identical on a linear scale. In this condition, the FLL will slowly drift its NCO output and then suddenly lock, or it will fail to lock entirely because the signal of interest has ceased. For example, suppose the signal of interest were modulated at a symbol rate of f_{sym} = 10 kHz instead of 50 kHz, and suppose the Doppler offset were a constant 30 kHz. Let additive white Gaussian noise be added to set the SNR to 20 dB (see Figure 10).

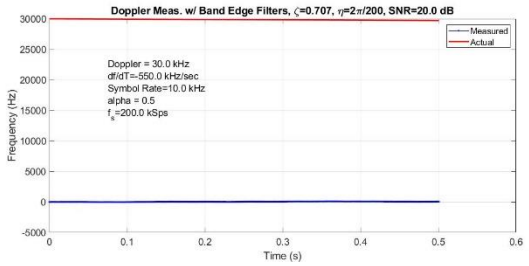

Figure 10: Failure of Band Edge Filter FLL When Doppler Exceeds Signal Modulated Bandwidth

In Figure 10, the measured frequency fluctuates around 0 Hz, never approaching the actual frequency offset. If the Doppler offset of the signal were small enough so that its spectrum intersected with the main lobe of one of the band edge filters, the energy imbalance would spur the control loop back into action and the FLL would eventually lock onto the Doppler. Similarly, if the Doppler offset caused the incoming signal to be outside of both band edge filters' main lobes, but it excites the nearest sidelobes of only one of the band edge filters, the FLL will lock slowly. At first, the energy difference between the band edge filters is very small, so the FLL applies the frequency correction. Suddenly, the signal is pushed into one of the band edge filter's main lobes, and the error magnitude dramatically increases, causing the FLL to lock quickly. This can be illustrated with an example similar to the previous scenario, except the Doppler offset is 19.5 kHz (see Figure 11) and is held constant.

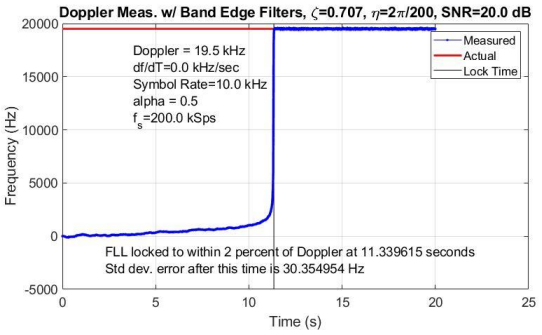

Figure 11: Performance of Band Edge Filter FLL When Doppler Offset Excites Nearest Sidelobes of Only One Band Edge Filter

Mitigation of Band Edge FLL Disadvantage

A simple modification to the design allows it to acquire and track large Doppler offsets. If the band edge filters are replaced with half-band filters and separated from each other by half the sample rate (placed at $\pm f_s/4$), then at least one of the filters will always capture energy from the incoming signal regardless of the Doppler offset. Figure 12 shows an upper band edge filter occupying the

positive frequencies and a lower band edge filter occupying the negative frequencies. For comparison, both band edge filters' spectra are plotted against the matched filter used to shape the baseband data in the transmitter.

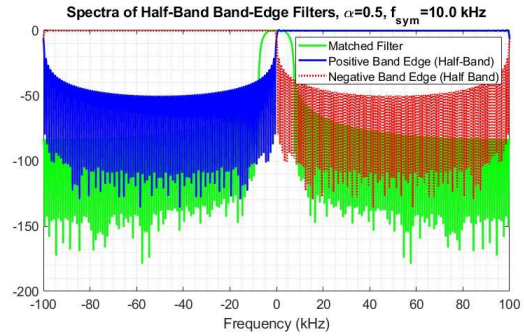

Figure 12: Spectra of Half-Band Band Edge Filters and Matched Filter

With these new band edge filters, the scenario of Figure 10 was re-simulated with the added imperfection of a time changing Doppler of -550 Hz/s. This time, the 30 kHz offset was detected quickly (see Figure 13), but the FLL needed nearly 27 milliseconds to achieve lock.

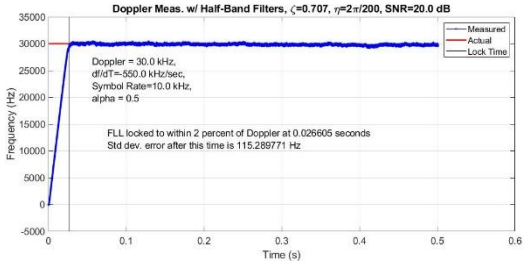

Figure 13: Success of Half-Band Band Edge Filter FLL When Doppler Exceeds Modulated Bandwidth

The standard deviation of the frequency error after lock in this example is comparable to the scenario of Figure 7, which was the 20 dB SNR simulation of a 12.5 kHz Doppler. However, a proper comparison between this half-band band edge FLL and Harris' optimum design requires a re-simulation of the scenario of Figure 7 in order to make a direct comparison of performance. The half-band band edge FLL was re-simulated with a 12.5 kHz Doppler offset changing at -550 Hz/s. Figure 14 shows that the standard deviation of the frequency error after lock is worse than it was with the optimum band edge FLL design. The versatility of the half-band filters comes at a cost of increased frequency error magnitude.

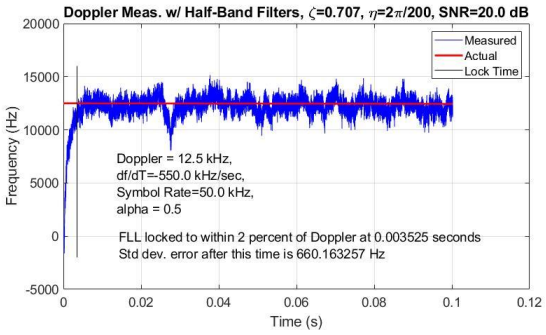

Figure 14: Performance of Half-Band Band Edge Filter FLL at SNR = 20dB

We can recover the benefits of the optimum design and retain the locking capability of the half-band design if we construct our band edge filters to be numerically equal to the sum of an optimum filter and a half-band filter, and scaled so that they have a maximum gain of unity. This change does not alter the structure of the block diagram of the FLL, it only replaces the coefficients of the band edge filters. Figure 15 shows the spectra of the hybrid half-band optimum band edge filters. Figure 16 shows that when it is tested with a 12.5 kHz Doppler for a 50 kHz BPSK signal, its frequency error is lower than the half-band's but higher than the optimum. Figure 17 shows that it can still lock onto the 30 kHz Doppler offset (for a 10 kHz modulated signal), although it takes more time to do so than the half-band FLL.

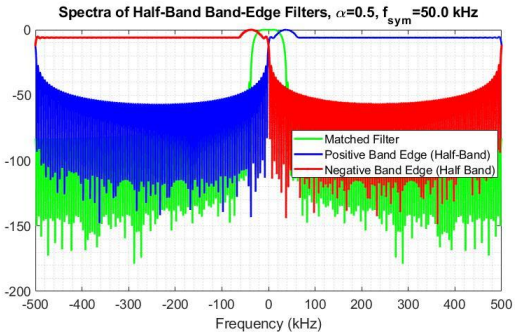

Figure 15: Spectra of Hybrid Half-Band and Optimum Band Edge Filters and Matched Filter

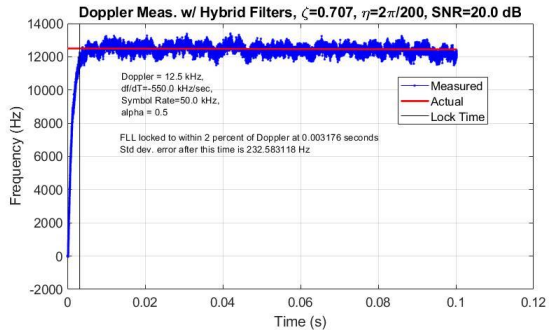

Figure 16: Demonstration of Hybrid Band Edge FLL Locking onto Doppler Within f_{sym}

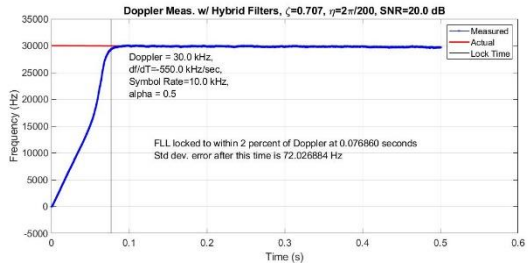

Figure 17: Demonstration of Hybrid Band Edge FLL Locking onto Doppler Beyond f_{sym}

DELAY AND MULTIPLY DEVICES

Background

Prefiltered delay and multiply structures have been designed to determine unknown symbol rates for phase modulated signals.[2,3] In his paper, Kuehls shows that for a delay that is less than a symbol time period, the product of a filtered BPSK signal with a delayed version of itself contains a periodic term with a baseband spectrum related to the symbol rate of the received signal.[2] A modified version of Kuehls' derivation can show that this term is multiplied by a carrier with twice the frequency offset.

Let incoming signal *s(t)* be a BSPK signal with symbol rate $f_b = 1/T$ and frequency offset f_0. It is constructed in the transmitter using a baseband pulse *p(t)* in order to band-limit the signal. The received signal passes through a noise-reduction filter *h(t)* and becomes *c(t)*. Then, *c(t)* branches off into two paths, one of which is a delay of *d*. These branches are multiplied together to form *b(t)*.

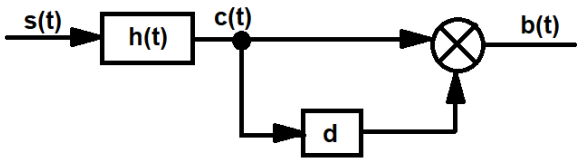

Figure 18: Delay and Multiply Device with Prefilter

$$s(t) = \sum_{n=-\infty}^{\infty} a_n p(t-nT) e^{j2\pi f_0 t} e^{j\theta} \quad (5)$$

$$c(t) = \sum_{n=-\infty}^{\infty} a_n q(t-nT) A e^{j2\pi f_0 t} e^{j\theta} e^{j\varphi}$$

The factor *A* represents a change in amplitude, and the $e^{j\phi}$ factor represents a phase change caused by the noise reducing filter *h(t)*. The expression *q(t)* represents the effect of the filter *h(t)* on the baseband pulse *p(t)*. The signal of interest, *b(t)* is the product of *c(t)* and *c(t-d)*.

$$b(t) = \left(\sum_{n=-\infty}^{\infty} \sum_{m=-\infty}^{\infty} a_n a_m q(t-nT) \cdot q(t-d-mT)\right) \cdot \left(A^2 e^{j2\pi 2 f_0 t}\right) \cdot \left(e^{-j2\pi f_0 d} e^{j2\theta} e^{j2\varphi}\right) \quad (6)$$

The first factor in parentheses, the double summation, can be broken down into two pieces: one for which *n=m* and one for which *n≠m*. The *n=m* term is periodic, and the *n≠m* term is random.[2] The periodicity of the *n=m* term is caused by the product of *q(t-nT)* and *q(t-d-nT)*. This product remains constant when the data symbol is the same as it was during the previous symbol period. However, when the data symbol changes, the delay ensures that the product also undergoes a change. The change can only happen on symbol time boundaries. This effect is readily seen in a simple case of a BPSK signal formed with rectangular pulses as in Figure 19.

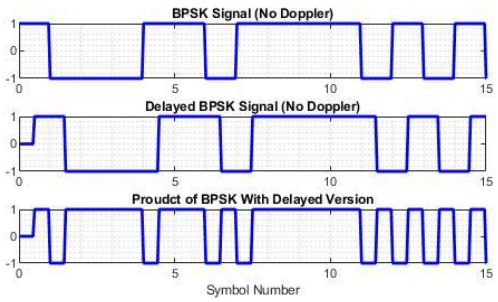

Figure 19: Forming Product of Rectangular-Pulsed BPSK Signal with Delayed Version of Itself

Here, the only possible values for the BPSK signal are +1 and -1, and the only possible values for the product of the signal and the delayed version are +1 when they agree and -1 when they disagree. In the general case, the transmitter's pulse shaping filter will round the edges in order to contain the spectrum. This tends to impart a small amplitude ripple on the "steady state" portion of the BPSK signal, and this ripple is also seen in the product of *q(t-nT)* and *q(t-d-nT)*. However, even in this more general case, most of the change exhibited in this product occurs when the data changes. Figure 20 shows the same data sequence from the previous figure but with rounded edges. A small ripple can be seen in the lower subplot representing the product of the signal and its delayed version. Larger changes in the product occur in symbols 6 through 10 when the BPSK sequence

alternates back and forth. The largest changes in the product occur at the beginning and ending of a run of consecutive +1's or -1's. Regardless, these changes occur at boundaries of the symbol time, demonstrating that this product is periodic.

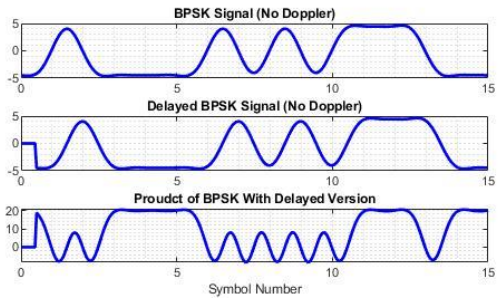

Figure 20: Forming Product of Filtered BPSK Signal with Delayed Version of Itself

For the purposes of this paper, the second factor in parenthesis of (6) is of interest because it contains the Doppler frequency offset information we are seeking. The third factor of (6) consists of a phase constant. Since the original signal *s(t)* is BPSK modulated, the product of a_n^2 is equal to 1.

The spectrum of *b(t)* depends on the shaping used in the transmitter and the time delay between the signal and its delayed version. If the BPSK signal consists of rectangular pulses (no shaping filter), then the delay-multiply device spectrum will show the tone at twice the Doppler offset surrounded by equal-amplitude tones separated by the symbol rate, as in Figure 21. A close-up of the largest tone is shown in Figure 22.

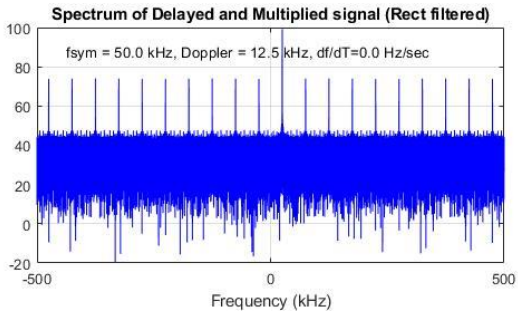

Figure 21: Spectrum of Rectangular Shaped BPSK Signal Passed Through Delay-Multiply Device (f_{sym} = 50 kHz, Doppler = 12.5 kHz)

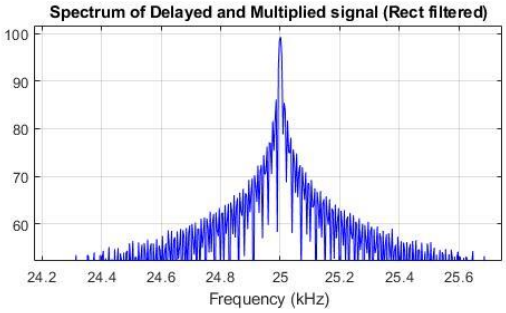

Figure 22: Close-up of Largest Tone of Figure 21 at Twice Doppler Frequency Offset

When the delay is varied between zero and the symbol period, the spectrum emphasizes different symbol rate tones. The example below shows a 50 kHz Doppler on a BPSK signal modulated at a symbol rate 50 kHz captured at 1 MS/s per second (20 samples per symbol). The delay element is varied between zero and 19 samples of delay, and the resulting spectrum is plotted in a separate subplot window. Observe that when the delay is set to zero, the symbol rate lines are not present. Furthermore, the peak we are interested in that is located at 100 kHz (twice the Doppler frequency) diminishes in amplitude as the delay is varied. If the delay were set to the symbol rate, 20 samples in this case, the Doppler tone would be completely absent. If our goal were to obtain a symbol timing reference instead of locking onto the Doppler offset, this would be the best delay choice.

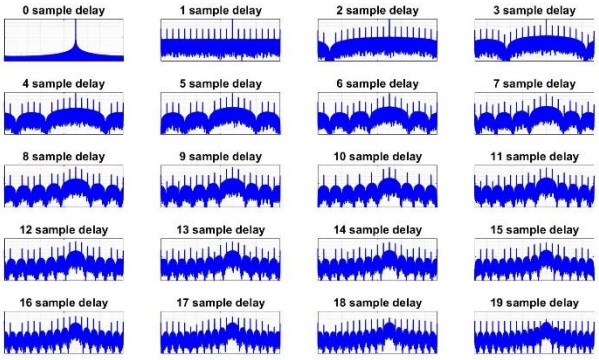

Figure 23: Spectrum of Delay-Multiply Output for BPSK with 50 kHz Doppler, Rectangular Shaping, Varying Delay from 0 Samples to 19 Samples

If the BPSK signal is shaped with a root raised cosine filter in the transmitter, the delay-multiply device exhibits a spectrum with three primary tones: the tone at twice the Doppler frequency, and the symbol rate tones on either side of it. Once again, the delay affects the spectrum and allows emphasis or de-emphasis of the Doppler tone (see Figure 24).

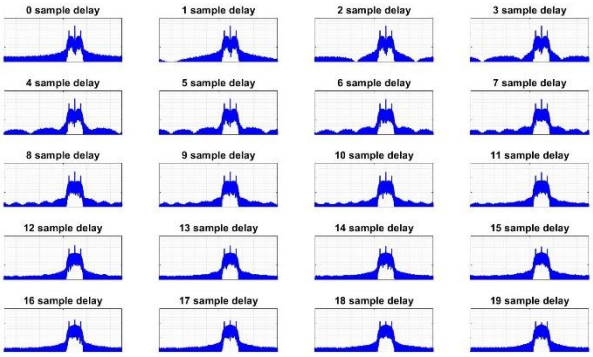

Figure 24: Spectrum of Delay-Multiply Output for BPSK with 50 kHz Doppler, Root Raised Cosine Shaping, Varying Delay from 0 Samples to 19 Samples

Incorporation of Delay-Multiply Device into FLL

The structure of the delay-multiply FLL is similar to the band edge FLL. The incoming signal is filtered with noise reducing filter *h(t)*. The product of the signal with a delayed version of itself is formed. The change in angle of this product with respect to the previous value is computed and the result is passed to the proportional-integral filter, which in turn feeds an NCO. The NCO output is conjugated, and the result is multiplied with the incoming signal, completing the feedback loop. This block diagram is shown in Figure 25.

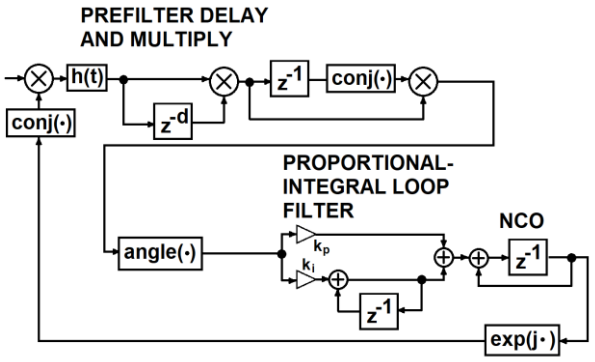

Figure 25: Delay-Multiply FLL for BPSK Signals

Performance of Delay-Multiply Device FLL

The delay-multiply FLL of Figure 25 was simulated with a BPSK signal modulated at 50 kHz and filtered with a square root raised cosine filer with α = 0.5. The delay element was set to one sample, and the sample rate was 1 MS/s. The noise reducing filter *h(t)* was assigned to be a half-band filter. It was observed that using the same values for ζ and η as the band edge filter FLL produced large frequency errors in the 5-6 kHz range along with extremely small lock times on the order of 50 microseconds. Therefore, a search was conducted for a set of parameters that produce similar lock times as the band edge filter FLL under similar SNR and Doppler offset conditions. It was determined that $\zeta = 1/\sqrt{40}$ and $\eta = 2\pi/(200\sqrt{20})$ produce similar lock times. The FLL proportional and integral gain terms were set by equation (4) using these values. The Doppler was set to be initialized at 12.5 kHz and changing at a rate of -550 Hz/s. Noise was added to make the SNR equal to 20 dB. This is the same scenario depicted in Figure 7 for the band edge filter FLL. The result for the delay-multiply FLL is shown in Figure 26. The delay-multiply FLL's measured frequency at SNR = 20 dB is significantly noisier than the measurement from the band edge filter FLL. The standard deviation was more than 7 times that of the band edge filter's measurement. This simulation was re-run with the SNR set to 5 dB, and the result is shown in Figure 27. At 5dB SNR, the variation in the delay-multiply FLL's measured frequency is nearly triple the value of the band edge filter FLL's result from Figure 8.

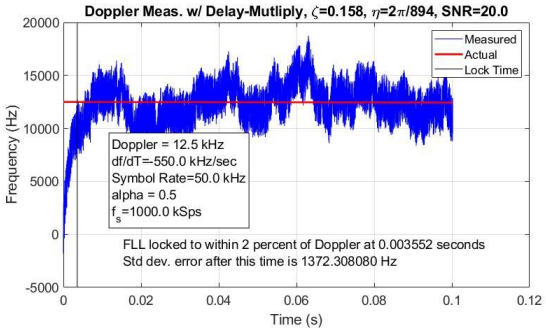

Figure 26: Performance of Delay-Multiply FLL at SNR = 20 dB

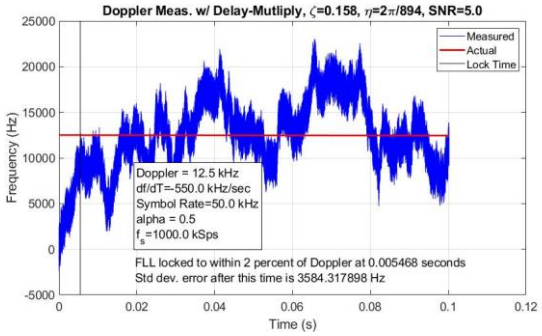

Figure 27: Performance of Delay-Multiply FLL at SNR = 5 dB

If we adjust the loop bandwidth and damping parameters to η = $2\pi/2828$ and $\zeta = 1/\sqrt{400}$, the frequency error variation will be reduced to approximately the level seen in Figure 8 for the band edge filter FLL's 5-dB scenario. However, the delay-multiply FLL will require more time to achieve lock. The 5-dB scenario from the previous

figure was re-run as Figure 28 using these parameter values. A comparison between Figure 28 with Figure 8 shows that the delay-multiply FLL now has a standard deviation of 1159.3 Hz after lock compared to the band edge filter FLL's 1272.0 Hz. However, the delay-multiply FLL requires 130 milliseconds to achieve lock compared to the band edge filter's 2.99 milliseconds. No matter how the damping and loop bandwidth parameters are adjusted, the delay-multiply FLL cannot simultaneously match the band edge filter FLL's performance of lock time and frequency error after lock.

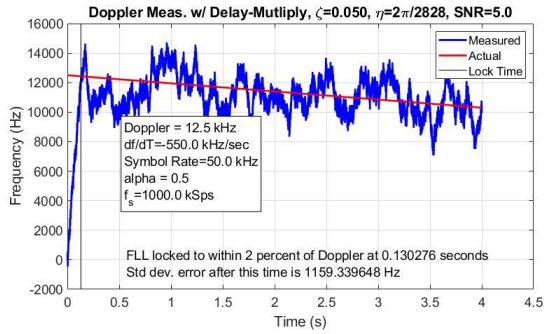

Figure 28: Performance of Delay-Multiply FLL at SNR = 5 dB with Reduced Loop Bandwidth

Advantages of Delay-Multiply Device FLL

With only a single filter, a working delay-multiply FLL can be built with fewer field programmable gate array logic resources than a band edge filter FLL. The noise reducing filter should have a passband of no more than $\pm f_s/4$ for BPSK. Figure 29 shows the delay-multiply FLL locking onto a time-varying Doppler initially at one quarter of the sample rate and changing by -550 Hz/s. The FLL is able to lock in less than 15 milliseconds.

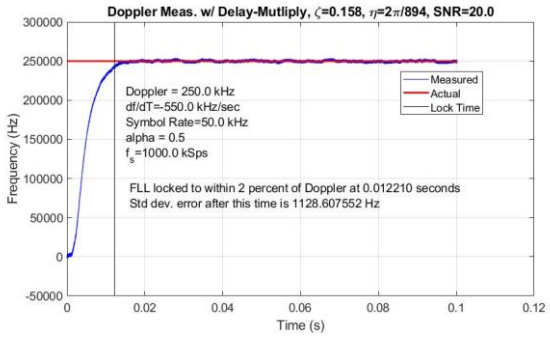

Figure 29: Performance of Delay-Multiply FLL with Doppler Offset Initially at $f_s/4$

Disadvantages of Delay-Multiply Device FLL

The most obvious disadvantage of the delay-multiply FLL is that its accuracy does not match the accuracy of the band edge filter running under the same SNR conditions and the same loop bandwidth parameters. The derivation of the delay-multiply expression hinted at another major disadvantage. The *n=m* term of equation (6) contains the factor a_n^2, which is equal to 1 for BPSK. If the incoming signal were modulated with QPSK instead, this factor does not simplify. Instead, the output of the prefilter *h(t)* must be squared before the resulting signal is delayed and multiplied. This step creates the factor a_n^4, which is 1 for QPSK. While this alteration restores the simplification of equation (6), it also pushes the maximum spectral tone to four times the Doppler frequency instead of two times because it creates the factor $(A^4 e^{j2\pi 4 f_0 t})$. In addition, the delay-multiply FLL would be limited to detecting Doppler frequencies in the range $\pm f_s/8$ for QPSK instead of $\pm f_s/4$.

CLOSING REMARKS

Band edge filters provide an effective way to measure and correct time-varying Doppler for a variety of phase modulated formats. A modified version of the band edge filter preserves this capability while extending the frequency correcting range. Filter implementations tend to consume logic resources in field programmable gate array designs, so it is useful to consider alternatives to the band edge filter FLL that require fewer filters. Prefilter delay and multiply techniques offer an alternative that can avoid the implementation of filters at the cost of reduced accuracy and limited frequency correcting range.

APPENDIX

A stable second-order analog phase-locked loop has a denominator with the structure shown in (A.1).

$$\frac{\theta_o(s)}{\theta_i(s)} = \frac{numerator}{s^2+2\zeta\omega_n s+\omega_n^2} \qquad \text{(A.1)}$$

The digital phase-locked loop with proportional constant k_p and integral constant k_i has a block diagram shown in Figure 30 and a transfer function as expressed in (A.2).

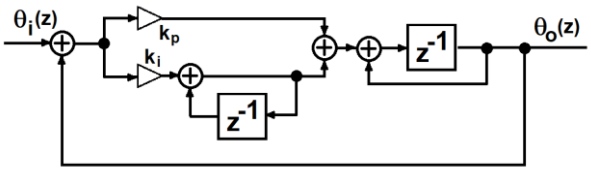

Figure 30: Second Order Digital Phase Locked Loop

$$\frac{\theta_o(z)}{\theta_i(z)} = \frac{(k_p+k_i)z-k_p}{z^2+(k_p+k_i-2)z+(1-k_p)} \qquad \text{(A.2)}$$

In this derivation, the goal is to find a relationship between the proportionality constants k_p and k_i, the analog damping factor ζ, and the natural damping

frequency ω_n. Our starting point is to replace the denominator of the analog system of (A.1) with an equivalent digital domain expression. The bilinear transform relating *s* to *z* is shown in (A.3).

$$s = \frac{2}{T_s}\left(\frac{z-1}{z+1}\right) \tag{A.3}$$

In (A.3), the sample period is T_s. Substituting the bilinear transform expression into (A.1) produces a new expression in terms of *z* as shown in (A.4).

$$\frac{\theta_o(z)}{\theta_i(z)} = \frac{numerator}{\left(\frac{z-1}{z+1}\right)^2 + 2\zeta\left(\frac{\omega_n T_s}{2}\right)\left(\frac{z-1}{z+1}\right) + \left(\frac{\omega_n T_s}{2}\right)^2} \tag{A.4}$$

Replacing the ratio $\omega_n T_s/2$ with η and multiplying the numerator and denominator by $(z+1)^2$, yields (A.5).

$$\frac{\theta_o(z)}{\theta_i(z)} = \frac{numerator}{(z-1)^2 + 2\zeta\eta(z+1)(z-1) + \eta^2} \tag{A.5}$$

Next, we combine powers of z in the denominator of (A.5) and compare the result to (A.2).

$$\frac{\theta_o(z)}{\theta_i(z)} = \frac{numerator}{z^2 + z\left(\frac{2\eta^2-2}{1+2\zeta\eta+\eta^2}\right) + \left(\frac{1-2\zeta\eta+\eta^2}{1+2\zeta\eta+\eta^2}\right)} \tag{A.6}$$

Comparing (A.6) to (A.2), produces two equations with two unknowns:

$$1 - k_p = \frac{1-2\zeta\eta+\eta^2}{1+2\zeta\eta+\eta^2} \tag{A.7}$$

$$k_p + k_i - 2 = \frac{2\eta^2+2}{1+2\zeta\eta+\eta^2}$$

Solving (A.7) for k_p and k_i completes the derivation, with the result in (A.8)

$$k_p = \frac{4\zeta\eta}{1+2\zeta\eta+\eta^2} \tag{A.8}$$

$$k_i = \frac{4\eta^2}{1+2\zeta\eta+\eta^2}$$

Acknowledgments

The authors wish to acknowledge NIWC Pacific's Naval Innovative Science and Engineering (NISE) program for funding and supporting the project that led to this paper.

References

1. Harris, F., "Band Edge Filters: Characteristics and Performance in Carrier and Symbol Synchronization," Proceedings of the 13th International Symposium on Wireless Personal Multimedia Communications, Recife, Brazil, October 11-14, 2010.
2. Kuehls, J.F. and E. Geraniotis, "Presence Detection of Binary-Phase-Shift-Keyed and Direct-Sequence Spread-Spectrum Signals Using a Prefilter-Delay-and-Multiply Device," IEEE Journal on Selected Areas in Communications, vol. 8, No. 5, June 1990.
3. Chan, Y.T., B. H. Lee, R. Inkol, and F. Chan, "Estimation of Symbol Rate from the Autocorrelation Function," 2009 Canadian Conference on Electrical and Computer Engineering, St. John's, NL, Canada, May 3-6, 2009.